JOURNAL OF THE ENGINEERING MECHANICS DIVISION

FINITE ELEMENT ANALYSIS OF WAVE DIFFRACTION BY A CRACK

By Zdeněk P. Bažant,[1] M. ASCE, John L. Glazik, Jr.,[2] and Jan D. Achenbach[3]

STATEMENT OF PROBLEM

One problem of considerable interest in fracture mechanics of brittle elastic solids is that of fracture induced by elastic waves. To decide whether a given incoming wave will make a crack propagate, it is necessary to calculate the time history of the stress intensity factor, which characterizes the strength of stress singularity at the crack tip. The problem has been recently approached analytically and some basic problems have been solved (2,3,31). The analytical solutions are, however, quite complicated, and analytical work seems hardly feasible for more involved geometries. A numerical approach is, therefore, inevitable for solving more complicated cases. The objective of this study is to explore application of the finite element method with step-by-step integration in time.

The general two-dimensional motion of an elastic continuum can be split into two independent motions: In-plane and antiplane. The in-plane motion is practically of greater interest, but the antiplane (shear) motion is simpler to analyze, while it contains many of the salient features of the in-plane motion. Therefore, antiplane wave motions in solids with cracks should be studied first and this paper will be devoted principally to this case.

The elastodynamic stress field around a straight crack of length $2a$ in an infinitely extending isotropic elastic medium will be studied. Let a crack in the xz plane of a Cartesian system be subjected to an anti-plane shear wave with a front parallel to the crack plane. The wave arrives from the positive y direction [Fig. 1(a)]. By virtue of superposition, the solution to this problem,

Note.—Discussion open until November 1, 1976. To extend the closing date one month, a written request must be filed with the Editor of Technical Publications, ASCE. This paper is part of the copyrighted Journal of the Engineering Mechanics Division, Proceedings of the American Society of Civil Engineers, Vol. 102, No. EM3, June, 1976. Manuscript was submitted for review for possible publication on September 11, 1975.

[1]Prof. of Civ. Engrg., Northwestern Univ., Evanston, Ill.
[2]Grad. Student, Northwestern Univ. Evanston, Ill.
[3]Prof. of Civ. Engrg., Northwestern Univ., Evanston, Ill.

$\bar{w}(x, y, t)$, can be decomposed into parts, $\bar{w}(x, y, t) = w_A(x, y, t) + w_B(x, y, t)$, in which $w_A(x, y, t)$ is the incoming wave propagating as if no crack existed; and $w_B(x, y, t)$ is the diffracted wave that is caused by a distributed tangential (antiplane) load, $S(x, t)$, on the crack surfaces [Fig. 1(b)], in which $S(x, t)$ is chosen such that it cancels the value of stress due to $w_A(x, y, t)$ at the

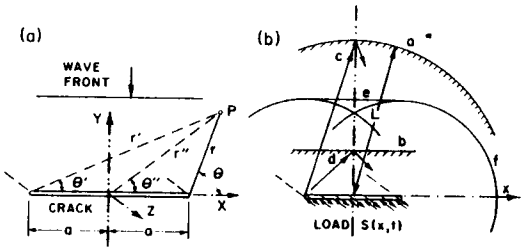

FIG. 1.—(a) Crack Subjected to Antiplane Shear Wave; (b) Planar Wave (Front e), Cylindrical Wave (Front f), and Spurious Reflections of Waves c and d from Finite Element System Boundaries a and b

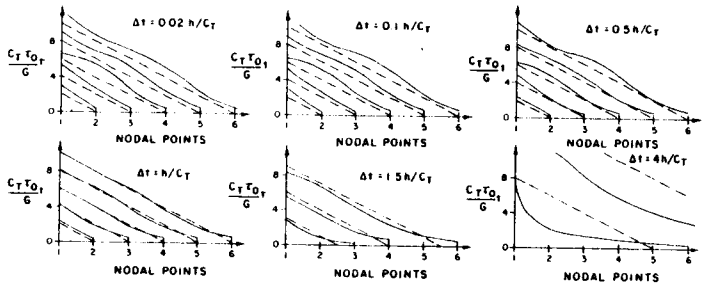

FIG. 2.—Results of Implicit Numerical Method (Solid Lines) and Exact Solution (Dashed Lines) for One-dimensional Shear Wave Using Various Time Steps

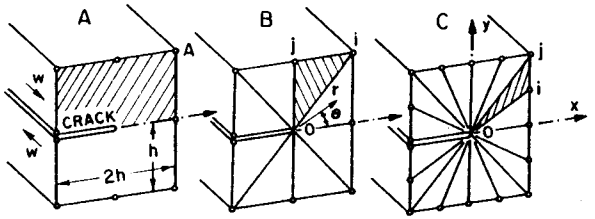

FIG. 3.—Singular Finite Elements with Constrained Nodes (A) and with Free Nodes (B and C)

location of the crack. Obviously, the mode III stress-intensity factor, K_3, is nonzero only in the solution $w_B(x, y, t)$, and, therefore, only this part of the solution is of interest for fracture. Here K_3 is defined as $\lim (\sqrt{2r}\,\tau_{yz})$ for $r \to 0$ at $\theta = 0$, in which r and θ are the polar coordinates in Fig. 1(a) and τ_{yz} is the Cartesian shear stress component.

In particular, a uniform load, $S(x,t)$, which is a Heaviside step function of time, $S(x,t) = SH(t)$, will be considered herein. The analytical solution to this problem is known for times shorter than the time that an antiplane disturbance needs to travel from one crack tip to the other, i.e., $t < 2a/c_T$. This solution is (3, p. 380)

$$K_3 = \frac{2}{\pi} S\sqrt{2c_T t} = \frac{4}{\pi} S\sqrt{a}\sqrt{\frac{c_T t}{2a}} \quad \ldots\ldots\ldots\ldots\ldots\ldots (1)$$

in which t = time; and c_T = shear wave velocity.

Some Problems in Finite Element Analysis of Elastic Wave Propagation

The finite element method reduces the elastodynamic problem with damping to the following second-order linear ordinary matrix differential equation in time:

$$\mathbf{M}\ddot{\mathbf{u}} + \mathbf{D}\dot{\mathbf{u}} + \mathbf{K}\mathbf{u} = \mathbf{F} \quad \ldots\ldots\ldots\ldots\ldots\ldots\ldots\ldots (2)$$

in which $\mathbf{u}$ = column matrix of all nodal displacement components; $\mathbf{F}$ = associated applied nodal force components; $\mathbf{K}$ = stiffness matrix; $\mathbf{M}$ = mass matrix; and $\mathbf{D}$ = damping matrix (which is zero in the present study, except when artificially introduced). There are currently many numerical step-by-step algorithms available for the integration of this equation of motion. Most work, however, has been concerned with vibrations. When dealing with wave propagation problems, some unexpected difficulties are encountered so that the numerical algorithms should be examined first.

Element Size for Implicit Step-by-Step Methods.—Consider the most simple test case: Plane shear waves propagating in an elastic half-space, $x \geq 0$, in the direction normal to the surface, $x = 0$. The wave is induced by a surface traction, $\tau_{xz} = \tau_0 H(t)$, in which τ_0 = constant; and $H(t)$ = Heaviside step function. The displacements of material points are $w(x,t) = (c_T\tau_0/G)(t - x/c_T)H(t - x/c_T)$, in which x = distance from the half-space surface; G = elastic shear modulus; c_T = shear wave speed = $(G/\rho)^{1/2}$; and ρ = mass density. The problem is one-dimensional and axis x is divided by uniformly spaced nodal points $i = 1, 2, 3 \ldots$, into constant strain finite elements of length h. A numerical solution was developed by using Anderson's version (4) of Newmark's β algorithm (23) (with $\beta = 0.25$), in which for time step (t_{i-1}, t_i) the increment, $\Delta\mathbf{u}_i$, is solved from the matrix equation

$$\mathbf{K}_i^*\Delta\mathbf{u}_i = \Delta\mathbf{F}_i^* \quad \ldots\ldots\ldots\ldots\ldots\ldots\ldots\ldots (3a)$$

$$\text{with} \quad \mathbf{K}_i^* = \mathbf{K}_i + \frac{2}{\Delta t}\mathbf{D}_i + \frac{4}{\Delta t^2}\mathbf{M}_i; \quad \Delta\mathbf{F}_i^* = \mathbf{D}_i\dot{\mathbf{u}}_{i-1} + \mathbf{M}_i\mathbf{A}_i + \mathbf{F}_i - \mathbf{R}_{i-1};$$

$$\mathbf{A}_i = \frac{4}{\Delta t}\mathbf{u}_{i-1} + \ddot{\mathbf{u}}_{i-1} \quad \ldots\ldots\ldots\ldots\ldots\ldots\ldots\ldots (3b)$$

The recursive relations

$$\mathbf{u}_i = \mathbf{u}_{i-1} + \Delta\mathbf{u}_i, \quad \dot{\mathbf{u}}_i = \frac{2}{\Delta t}\Delta\mathbf{u}_i - \dot{\mathbf{u}}_{i-1} \quad \ldots\ldots\ldots\ldots\ldots\ldots (4a)$$

$$\ddot{\mathbf{u}}_i = \frac{4}{\Delta t^2}\Delta\mathbf{u}_i - \mathbf{A}_i, \quad \mathbf{R}_i = \mathbf{R}_{i-1} + \mathbf{K}_i\Delta\mathbf{u}_i \quad \ldots\ldots\ldots\ldots\ldots\ldots (4b)$$

are then applied. Here subscripts $i-1$ and i refer to times t_{i-1} and t_i; $R_i = 0$ for $i = 0$. The preceding relations are also valid for time variable $\mathbf{K}$ and $\mathbf{D}$.

In Fig. 2 the results (solid lines) obtained by using Eqs. 3 and 4 with a lumped mass (and zero damping) are compared with the exact solution for various values of the ratio $c_T\Delta t/h$, Δt being the time step. It is not surprising to see that the time step, Δt, cannot exceed a certain limit, but it is noteworthy that Δt should not be too small either. It is seen that, although this algorithm possesses unconditional numerical stability, best accuracy is obtained when

$$h \approx c_T\Delta t \quad \ldots\ldots\ldots\ldots\ldots\ldots\ldots\ldots\ldots\ldots (5)$$

i.e., the element size should roughly equal the distance traveled by a disturbance during the time step. This corresponds to advancing along the characteristic of the wave equation. Obviously, Eq. 5 requires that for best accuracy all finite elements in the system be of roughly equal size. This is a rather undesirable limitation in problems with cracks, because the necessity of using small finite elements near the crack tip and keeping the element size constant throughout the system leads to a huge number of equations.

In many cases it is unavoidable that, for some elements, h is significantly less than $c_T\Delta t$. The additional error caused by this appears to cease getting worse as Δt decreases below $0.1\ h/c_T$; (see Fig. 2). Thus, the maximum error due to Δt being much less than h/c_T should have a constant ratio to h, and so by choosing a sufficiently fine subdivision it must be possible to obtain accurate results even for a grid with varying element sizes. However, the additional error due to the violation of Eq. 5 would undoubtedly require a vastly greater number of equations (for a fixed error limit). Such a situation will be inevitable to some extent in a planar (mode I) motion because there are two significantly different wave speeds (usually of ratio 1.5-2.5), and Eq. 5 cannot be satisfied for both of them at the same time.

When the propagating disturbance has a sharp front, the finite element solution is known to give spurious oscillation both behind and ahead of the correct location of the front. The error in Fig. 2 can be regarded as a result of these oscillations. If the wave front were not sharp, a much smaller error could be expected and time steps much smaller than h/c_T would probably be admissible. In vibration problems, accuracy only requires a sufficiently small Δt, but there is no limit on smallest possible Δt.

The condition in Eq. 5 has been also obtained for other implicit unconditionally stable numerical algorithms, such as the version of Newmark's β algorithm employed in the general purpose program NASTRAN (19), which differs from Eqs. 3 and 4 in that $\beta = 1/3$ is used rather than $1/4$, and the Wilson's θ method (6,38) which is based on the assumption of a linear variation of acceleration throughout the time step, Δt, while Newmark-type algorithms imply constant acceleration during Δt. The accuracy of these solutions has been slightly worse than the accuracy of those shown in Fig. 2, but the dependence of error on the ratio $c_T\Delta t/h$ was the same.

Problem of Nonreflecting Boundaries.—Another problem resulting from the necessity of using a finite element system of finite size is how to avoid spurious

wave reflection at the boundary of the system of finite elements. Special boundary conditions intended for this purpose have been proposed by Lysmer, et al. (18), and others. These boundary conditions are derived under the assumption that a plane wave is passing the boundary in the normal direction. Similar boundary conditions can be constructed for other types of waves, e.g., cylindrical waves. It seems, however, impossible to find nonreflecting boundary conditions that would prevent reflection for all types of waves at the same time. In the problem at hand, in addition to the plane wave, there is a diffracted cylindrical wave emanating from the crack tip. Such a wave would require a different set of nonreflecting boundary conditions. For the present case, which involves both a plane wave and a diffracted cylindrical wave, it has been tried numerically whether the nonreflecting boundary condition of Lysmer (18) would work at least as an approximation. This appeared generally to be possible only if the nodal spacing at the boundary was much smaller than the distance of the boundary from the source of the cylindrical wave, and if the wave direction nowhere deviated by more than approx. 15° from the normal to the boundary. [See case c as opposed to case d in Fig. 1(b)]. These conditions can be achieved by making the boundary of the finite element system a circle of radius L at least four times the half-crack length [Fig. 1(b)] and centered at the midlength of the crack. However, this size is too large and requires an unacceptably great number of elements. Moreover, such a large size is not necessary because the time, $T_1 \approx 2L/c_T$, required for any diffracted wave to travel to the boundary and back to the crack tip far exceeds the time period of interest, T_0. Consequently, the system size, L, was chosen in all numerical calculations as $L \approx c_T T_0/2$ depending on the desired T_0, in which c_T = shear wave velocity. Then, the type of boundary condition was irrelevant for the motion near the crack and the conditions of either free or fixed boundary could be used, yielding the same results. Thus, the idea of developing a nonreflecting boundary and using a smaller region was abandoned.

It has also been found that spurious wave reflections arise at the boundary of two finite elements of substantially different sizes. This occurs not only for the implicit algorithms, but also for the explicit algorithm considered in the sequel.

Singular Crack-Tip Elements in Static Problems

Owing to the stress singularity at the crack tip, a prohibitively large number of ordinary finite elements with polynomial interpolation functions is needed to obtain accurate static solutions (5,13,16,30). It has also been shown (32) that the error decreases with the element size as $O(\sqrt{h})$ rather than as $O(h^2)$ which occurs when singularities are absent. For this reason, various special "singular" finite elements have recently been developed for the region around a crack tip (1,7,8,9,10,11,12,16,20,24,25,26,28,33,34,35,39,40). Quite simple and efficient singular elements for planar problems have been derived by Walsh (35) and these were refined in Ref. 7. A slightly different element was analyzed by Benzley and Beisinger (9) and by Tracey and Rice (28,33,34). These two formulations have served as the points of departure for the subsequent analysis.

The formulation of a singular finite element is based on the asymptotic near-tip displacement field. In the case of antiplane shear, this field is

$$w = \frac{K_3}{G}(2r)^{1/2}\sin\frac{\theta}{2} \quad \ldots\ldots\ldots\ldots\ldots\ldots\ldots\ldots\ldots\ldots (6)$$

in which r and θ = polar coordinates centered at the crack tip; ray $\theta = 0$ pointing in crack direction [Fig. 3(a)]; w = antiplane displacement (having direction z); G = shear modulus; and K_3 = mode III stress intensity factor. The derivation of the stiffness matrix will follow the procedure employed in Ref. 7 for planar (mode I) displacements.

Singular Elements with Constrained Nodes.—In addition to the singular field given by Eq. 1, for which K_3 may be regarded as a generalized displacement parameter, the singular element must also exhibit admissible rigid body motions (35). Further it must exhibit, as has been pointed out in Ref. 7, all homogeneous constant strain fields that can exist near the crack tip without any singular field. However, when attention is restricted to motions symmetric about axis x, the points on axis x are immobile and both rigid body motions and homogeneous strain states are negligible compared to the singular field near the crack tip. As an approximation, this condition may be assumed to exist over the whole singular element. Consequently, the column matrix of all generalized displacements of the singular element reduces in this particular case to a single variable, K_3. Furthermore, one may define column matrices of strain components, $\underset{\sim}{\epsilon} = [\partial w/\partial x,\ \partial w/\partial y]^T$, and of stress components, $\underset{\sim}{\sigma} = [\tau_{xz}, \tau_{yz}]^T$, in which superscript T denotes the transpose of a matrix. The relations of stresses and strains to displacements may now be stated as $\underset{\sim}{\epsilon} = \mathbf{B}K_3$, $\sigma = \mathbf{B}'K_3$, in which, according to Eq. 6

$$\mathbf{B} = \frac{1}{G}\sqrt{\frac{1}{2r}}\left[-\sin\frac{\theta}{2}, \cos\frac{\theta}{2}\right]^T, \quad \mathbf{B}' = \mathbf{GB} \quad \ldots\ldots\ldots\ldots\ldots\ldots (7)$$

The virtual work of stresses in the element on displacement variations $\delta\mathbf{u}$ within the area of the singular element may be expressed as $\delta W = \int_A (\delta\underset{\sim}{\epsilon})^T\sigma\, dA$, A being the area of the element. After substituting from Eq. 7, one obtains $\delta W = \int_A \delta K_3 \mathbf{B}^T\mathbf{B}' K_3\, dA = \delta K_3 k_0 K_3$, in which k_0 represents the stiffness coefficient associated with K_3:

$$k_0 = \int_A \mathbf{B}^T\mathbf{B}'\, dA = \int_0^{\pi}\int_0^{r(\theta)} \frac{1}{2G}\, dr\, d\theta \quad \ldots\ldots\ldots\ldots\ldots\ldots\ldots\ldots (8)$$

In the present case the stiffness matrix happens to reduce to a single number, k_0. Thus, the case of antiplane shear yields a very simple prototype of a singular element.

The displacements, w_i^B, at the boundary of the singular element are not free but are kinematically dependent upon a single parameter, K_3, according to the relations, $w_i^B = (K_3/G)(2r_i^B)^{1/2}\sin(\theta_i^B/2)$, in which r_i^B, and θ_i^B are polar coordinates of boundary nodes. The nodal equilibrium equations for the boundary nodes in the matrix of the finite element system must, therefore, be replaced by the foregoing relations between w_i^B and K_3.

To get a picture of the accuracy, a crack of length $2a$ (Fig. 4) in an infinite medium subjected at infinity to uniform antiplane shear stress $\tau_{yz} = S$ at planes parallel to the crack plane has been considered. The exact solution of stresses is given by Sneddon and Lowengrub (29) as

$$\tau_{yz} = \frac{r'' S}{\sqrt{r r'}} \cos\left(\theta'' - \frac{\theta}{2} - \frac{\theta'}{2}\right); \quad \tau_{xz} = \frac{r'' S}{\sqrt{r r'}} \sin\left(\theta'' - \frac{\theta}{2} - \frac{\theta'}{2}\right) \quad \ldots . \quad (9)$$

in which r, r', r'', θ, θ', and θ'' are shown in Fig. 1(a). The numerical solution was obtained using grids of the type shown in Fig. 5(a). (When the crack tip

TABLE 1.—Error in Static Crack Problem, as Percentage of Exact K_3

LOADING	AT INFINITY					CONSTANT STRAIN (ZERO K_3) LOADING							
Variable	w_p	K_3				Crack Loaded, K_3				Crack Fixed, K_3			
Element (1)	A (2)	A (3)	B (4)	C (5)	Ca (6)	A (7)	B (8)	C (9)	Ca (10)	A (11)	B (12)	Ba (13)	Ca (14)
h/a													
0.8	37.45	11.25	—	—	—	—	—	—	—	—	—	—	—
0.4	24.15	1.53	—	—	—	—	—	—	—	—	—	—	—
0.2	14.13	0.11	−16.69	—	—	—	—	—	—	—	—	—	—
0.1	7.71	−0.07	6.58	—	—	12.23	12.94	13.30	16.76	19.73	10.68	11.39	15.13
0.05	4.02	−0.10	—	—	—	—	—	—	—	—	—	—	—
0.025	—	—	—	—	—	—	—	—	—	—	—	−5.66	—
0.020	—	—	—	0.57	7.00	—	—	5.59	5.94	—	—	—	—

Note: Elements A, B, C from Fig. 3; Ba, Ca same as B, C, but with displacement continuity at edges.

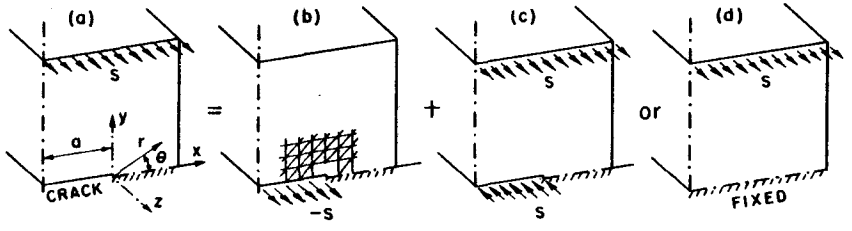

FIG. 4.—Decomposition of the Antiplane Problem for Loading at Infinity

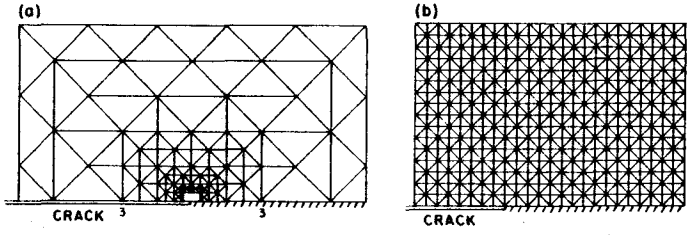

FIG. 5.—(a) Grid for Static Crack Problem (with Singular Element A, Fig. 3, of Size $h = a/20$); (b) Uniform Grid Used for Dynamic Problems (All Grids Used Were Similar Except for Element Size and Number of Degrees-of-Freedom)

element reached to line 3, e.g., the subdivisions enclosed by that line were, of course, deleted.) On the boundary of the domain in Fig. 5(a), the exact stress values given by Eq. 9 were considered as externally applied distributed loads. Constant strain triangular elements were used. They were arranged so as to decrease in size as the crack tip is approached [Fig. 5(a)], and numerical

solutions were obtained for various sizes h of the singular element, ranging from $h = 4a/5$ to $h = a/20$. The error in the stress intensity factor, K_3, is given in Table 1 (see columns for element A). Also given is the maximum error in displacements, which always occurs in point A ($\theta = 45°$, Fig. 3) at the boundary of the singular element. The correct values of displacements have been determined from strain values based on Eq. 9 using highly accurate numerical integration along a path beginning on the ray $\theta = 0$ (axis x).

From Table 1 (columns for element A) it is seen that the error diminishes quite rapidly with the element size, h. The values of K_3 have a very small error even for a relatively large singular element; around 0.1% for $h = a/5$. It is also noteworthy that for an extremely small element size the error ceases to diminish, and in order to further reduce the error the angular spacing of the boundary nodes of the singular element also would have to be diminished. However, the error in displacement is very large and even for a rather small singular element, $h = a/20$, the error is unacceptable (approx. 4%).

Obviously a singular element of this type is quite adequate for calculating the stress intensity factor, but not the displacements. Therefore, various ways of improving the accuracy of the displacements were explored.

Singular Elements with Free Nodes.—An obvious possibility to improve the values of displacements is to consider the displacements in the nodes around the crack tip to be independent rather than tied to the value of K_3. This has been done by Tracey and Rice (28,33,34). A similar approach in antiplane shear will now be considered. One may split the large single crack-tip element into a number of triangular elements forming a fan around the crack tip (elements B and C in Fig. 3) and enrich the singular strain field in each of these elements by a constant strain field. The constant strain field is, of course, not necessary for convergence, because for a sufficiently small crack-tip element it is always negligible with respect to the singular stress field. However, the enrichment by a constant strain field is needed to allow independent movement of all nodes of the element. The enriched antiplane displacement field within each element of the fan is

$$w = \mathbf{C}(x, y)\mathbf{w} + \left[\frac{1}{G}\sqrt{2r}\sin\frac{\theta}{2}\right] K_3; \quad \mathbf{w} = [w_0, w_i, w_j]^T \quad \ldots . \quad (10)$$

in which subscript 0 refers to the crack tip; and subscripts i and j refer to the other two nodes of the element in the fan (Fig. 3). Superscript T denotes a transpose and $\mathbf{C}(x, y)$ is a (1×3) row matrix. By differentiating Eq. 10, the column matrix of strains, $\underset{\sim}{\epsilon} = (\partial w/\partial x, \partial w/\partial y)^T$, is obtained in the form, $\underset{\sim}{\epsilon} = \mathbf{b}(x, y)\mathbf{w} + \mathbf{B}(r, \theta)K_3$, in which $\mathbf{b}(x, y)$ is a (2×3) matrix; and $\mathbf{B}$ is a column matrix given by Eq. 7. The virtual work of stress on displacement variations within the element is $\delta W = \int_A \delta \underset{\sim}{\epsilon}^T G \underset{\sim}{\epsilon}\, dA = \int_A (\delta \mathbf{w}^T \mathbf{b}^T + \delta K_3 \mathbf{B}^T) G (\mathbf{b}\mathbf{w} + \mathbf{B}K_3)\, dA$, which indicates that the (4×4) stiffness matrix of the triangular singular element with nodes 0, i, and j has the form

$$\mathbf{K} = \left[\begin{array}{c|c} \int_A \mathbf{b}^T G \mathbf{b}\, dA & \int_A \mathbf{b}^T G \mathbf{B}\, dA \\ \hline \int_A \mathbf{B}^T G \mathbf{b}\, dA & \int_A \mathbf{B}^T G \mathbf{B}\, dA \end{array}\right] \quad \ldots . \quad (11)$$

The elements of this matrix depending on **B** have been evaluated by Gaussian point numerical integration in the plane with Cartesian coordinates (r, θ), in which the triangular element appears as a rectangle. In contrast to the preceding large singular element with constrained nodes, displacements w_i, w_j are not tied to K_3 but are independent, so that the equilibrium equations associated with w_i, w_j need not be removed.

The results obtained with the fan of elements having free nodes (elements B and C in Fig. 3) are also shown in Table 1 for various sizes of the element and for various numbers of nodes at the boundary. However, although the values of nodal displacements around the crack tip have improved, the results for K_3 have gotten worse than those for the previous formulation (element A in Fig. 3).

The formulation just outlined lacks displacement continuity on the interfaces between singular and regular elements, except at the nodes. Benzley and Beisinger (9) removed such discontinuities by enriching the polynomial (bilinear) interpolation functions in the adjacent (transition) elements by a field that has K_3 as its parameter and coincides with the singular field in the nodes common with the crack-tip element, while gradually fading away over the transition element and reaching zero in the remaining nodes.

One is tempted to ask how much of the error might be due to the lack of full continuity. To explore this question, another variant of the aforementioned element was formulated by multiplying the singular term in Eq. 6 with the function $[1 - r/r_b(\theta)]^n$ in which $r_b(\theta)$ = the radial distance of the point at the boundary of the crack-tip element on the ray of angle θ; and n = a chosen constant. This function preserves the right singular field in the vicinity of the tip but makes the singular field vanish at the boundary with the adjacent elements, thus achieving displacement continuity. The stiffness matrix of this element was obtained by numerical integration in the plane with r, θ as Cartesian coordinates. However, the numerical results have not produced any clear improvement (see Table 1, Col. 10).

Dynamic Crack Problem with Singular Element

For dynamic analysis, it is necessary to derive also the mass (or inertia) matrix of the crack-tip element. One possible formulation is the consistent mass matrix, derived from the displacement interpolation functions. To obtain this matrix, the virtual work of inertia forces $\rho \ddot{w}$ (in which ρ = mass density; and superimposed dots denote time derivatives) over the element may be expressed as $\delta W = \int_A \rho \ddot{w} \delta w \, dA$. Denoting by **C** the row matrix that expresses w in terms of nodal displacements **u**, i.e., $w = \mathbf{Cu}$, one has $\delta W = \int_A \rho \, \delta \mathbf{u}^T \mathbf{C}^T \mathbf{C} \ddot{\mathbf{u}} \, dA$. This indicates that the consistent mass matrix of the singular element is $\mathbf{M} = \int_A \rho \mathbf{C}^T \mathbf{C} \, dA$. For the special case of the singular element with constrained nodes (Type A in Fig. 3, Eq. 8), **u** equals K_3, **C** is given by Eq. 6, and **M** reduces to a single number:

$$m = \frac{2\rho}{G^2} \int_\theta \int_r \left(r \sin \frac{\theta}{2} \right)^2 dr \, d\theta \quad \ldots\ldots\ldots\ldots\ldots\ldots\ldots\ldots\ldots\ldots \quad (12)$$

The time history of K_3 was calculated using the grid in Fig. 5(*a*) with 856

degrees-of-freedom, a singular element of size $h = a/20$, and a consistent mass matrix given by Eq. 12. The results are indicated by curve b in Fig. 6(*a*) in comparison with the exact solution (curve a, Eq. 1). It is seen that the solution obtained is much too low in magnitude, although the general trend is correct. The error might be caused by the fact that the singular element has twice the size of the adjacent elements, which violates the condition in Eq. 5. Since all displacements in this element are proportional to a single parameter, any disturbance is transmitted across the element instantaneously, and because the total inertia force associated with the whole element is large, the obtained growth of K_3 is too small. It has been checked whether any significant improvement can be achieved by using a consistent mass matrix for the singular element

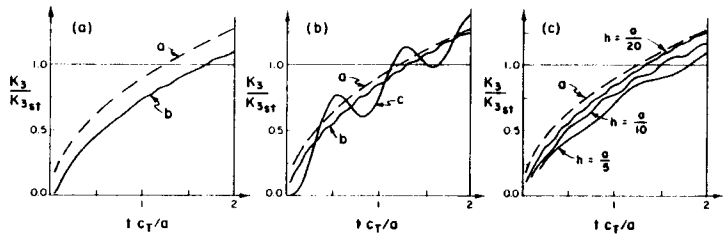

FIG. 6.—K_3 Histories (Solid Lines) Obtained by Implicit Method Compared to Exact Elastodynamic Solution (Dashed Lines): (*a*) for Element A, Fig. 3, Size $h = a/20$; (*b*) for Element B, Fig. 3, Size $h = a/20$ with Lumped Mass Matrix (curve b) and Consistent Mass Matrix (curve c); (*c*) for Various Sizes of Element B, Fig. 3

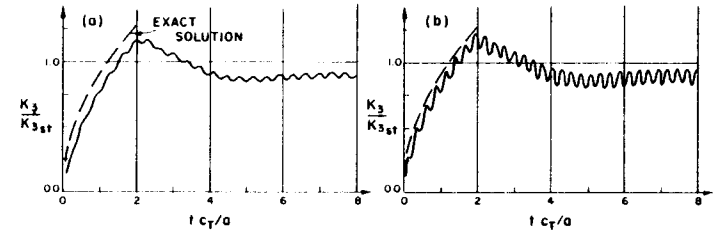

FIG. 7.—K_3 History after Arrival of Waves from Opposite Crack Tip: (*a*) Implicit Method; (*b*) Explicit Method Using Element B, Fig. 3 of Size $h = a/10$

and a lumped one for all other elements; but the accuracy was as poor as that obtained with consistent mass for all elements.

The aforementioned difficulties may be alleviated by using the fan of triangular singular elements with free nodes as described previously (elements B and C in Fig. 3). The consistent mass matrix for these singular elements has been derived similarly to Eq. 12, and numerical results have been obtained [curve c in Fig. 6(*b*)]; but they exhibit huge spurious oscillations. Yet, the average trend was much better than that obtained in the previous approach. Subsequently, the consistent mass matrix was replaced by the lumped mass matrix, which has zero coefficients associated with K_3. This has vastly improved the numerical results [curve b, Fig. 6(*b*)]. In retrospect, it appears to be a general rule that

only the lumped mass matrix should be used in wave propagation problems. The reason is that the finite element method implies simultaneous motion all over the element for each displacement mode, but this is possible only in a medium of zero mass in which disturbances propagate with infinite velocity. To be consistent with this fact, the mass must be lumped into the nodes. Thus, the lumped mass matrix appears to be theoretically more "consistent" than the so-called consistent mass matrix.

Using a lumped mass matrix and the fan of singular triangular elements with free nodes (element B in Fig. 3), numerical solutions were obtained for various sizes of the finite elements [see Fig. 6(*c*)]. The solution appears indeed to converge to the exact one [curve a in Fig. 6(*c*)] as the element size decreases.

The exact solution given by Eq. 1 is limited to the time before the wave diffracted from one crack tip arrives at the opposite tip, i.e., $t \leq 2a/c_T$. The finite element model developed herein is one means of extending the solution in time. To avoid spurious wave reflections at the boundary, the size of the region must be increased accordingly. Element size $h = a/10$ was chosen as the maximum acceptable for sufficient accuracy [Fig. 6(*c*)]. For the size of the region that is needed for the time period, $t < 8a/c_T$, a grid leading to a symmetric system of 2,092 equation of half-band width 85 was obtained. This system had to be solved 80 times in 80 time steps to reach the time desired.

The requirements for computer storage, as well as computer time, are quite large, and to reduce these requirements, direct solution of the equation system by Gaussian elimination has been abandoned. Instead, compact storage with a pointer matrix and Gauss-Seidel iteration were used to solve the equations. In the present problem, the iterations converged extremely rapidly. After experimenting with the overrelaxation factor, the factor of 1.15 was found to be optimum. By contrast, in static problems values between 1.8 and 1.9 are known to be best. The number of iterations necessary for the relative change of the sum of absolute values of all unknowns in the last iteration to be less than 0.1% was only seven to nine, while in a static problem for the same grid hundreds of iterations would be necessary to solve a system of 2,092 equations. The extremely rapid convergence is due to some extent to the fact that the values of unknowns from the previous step are good starting values for the iterative solution. The main reason for the rapid convergence is that the contribution of mass matrix **M** predominates in **K***, as given by Eq. 3*b*. Because the mass is lumped, this contribution appears only in the diagonal terms, making them prevalent by far over all other terms of the equations. Consequently, it appeared that the iterative method of solution not only allows a reduction in storage requirements but also considerably reduces the running time (80 time steps took approx. 9 min CPU time on CDC 6400 computer).

At the time, $t = t_1 = 2a/c_T$, when the first diffracted wave from the opposite crack tip arrives, the value of K_3 reaches a peak and subsequently declines, as expected. At the time, $t = t_2 = 2t_1$, a second diffracted wave arrives from the opposite crack tip and a third diffraction occurs. The approximate analysis carried out in Ref. 31 indicates that after time t_2 the solution of K_3 should again rise, although slower than before. However, the numerical solution [Fig. 7(*a*)], rather than rising, remained essentially constant after t_2. It did not even reach the correct static value, $K_3 = K_{3st}$. The cause of this discrepancy will be examined at the end of this section.

From the preceding analysis it is apparent that in wave diffraction situations an extremely small singular finite element (at least $h = a/100$) must be used. However, to achieve a manageable size of the system of equations, the element size must then be increased away from the crack tip, in violation of the condition

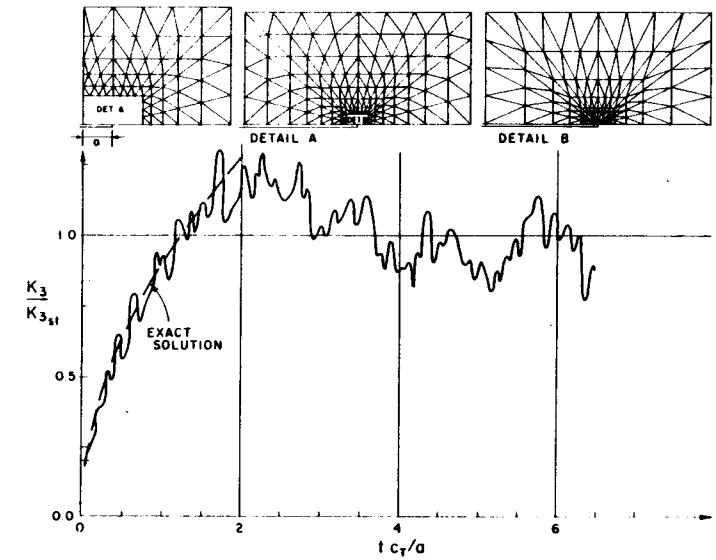

FIG. 8.—K_3 History after Arrival of Waves from Opposite Crack Tip, Obtained by Explicit Method and Grid Shown Using Element C, Fig. 3 (of Size $h = a/100$ and with 16 Rather Than 8 Elements Surrounding Crack Tip)

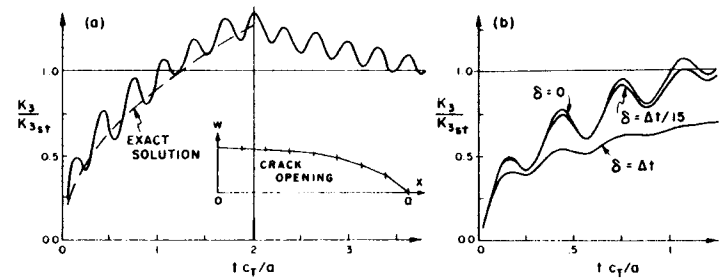

FIG. 9.—(*a*) K_3 History Obtained by Explicit Method with Nonsingular Calibrated Crack-Tip Elements and Regular Grid from Fig. 5(*b*); (*b*) Effect of Artificial Damping on Numerical Results (Diagonal Damping Matrix is Equal to δ times Diagonal of Stiffness Matrix)

in Eq. 5. Consequently, the implicit algorithm cannot be used and the only possibility is an explicit algorithm, which is feasible because here **M** and **D** are diagonal matrices. The explicit algorithm used has error $O(\Delta t^2)$ and is defined by the recursive relations for time step (t_i, t_{i+1}):

$$\dot{\mathbf{u}}_{i+1} = \left[\mathbf{F}_i - \mathbf{K}\mathbf{u}_i + \dot{\mathbf{u}}_i\left(\frac{1}{\Delta t}\mathbf{M} - \frac{1}{2}\mathbf{D}\right)\right]\left(\frac{1}{\Delta t}\mathbf{M} + \frac{1}{2}\mathbf{D}\right)^{-1};$$

$$\mathbf{u}_{i+1} = \mathbf{u}_i + \dot{\mathbf{u}}_{i+1}\,\Delta t \quad (13)$$

This algorithm is stable only for $\Delta t < h/c_T$. Numerical trials similar to those with the implicit algorithms (Fig. 2) were carried out, and it appeared that for the same accuracy the time step should be about 10 times less than that for the implicit method, i.e., $\Delta t \approx 0.1\ h/c_T$. However, calculation of one time step with the explicit algorithm is about 10 times cheaper, and so the cost of numerical solution is about the same. In contrast to implicit methods, however, the time step of the explicit method of Eq. 13 may be smaller than the aforementioned value without any loss in accuracy (except for the round-off error). Thus, the explicit method allows a grid of varying element size, provided *the time step is chosen according to the smallest element size in the system.*

After completion of the present study, distinctly more accurate numerical results have been obtained in other wave propagation problems by applying another explicit numerical algorithm which uses $\mathbf{u}_{i-1}$ instead of $\dot{\mathbf{u}}_i$ and is given by the recursive relation, $\mathbf{u}_{i+1} = [\mathbf{D}(2\Delta t)^{-1} + \mathbf{M}(\Delta t)^{-2}]^{-1}\{(2\mathbf{M}(\Delta t)^{-2} - \mathbf{K})\mathbf{u}_i + [\mathbf{D}(2\Delta t)^{-1} - \mathbf{M}(\Delta t)^{-2}]\mathbf{u}_{i-1} + \mathbf{F}_i\}$. With this algorithm, which has an error, $O(\Delta t^3)$, and is analogous to a method used in finite differences (15) (with $\Delta t \le h/c_T$ required for stability and $\Delta t = h/c_T$ being optimum), the solutions shown in figures herein would have been undoubtedly more accurate for the same computer cost.

The explicit algorithm from Eq. 13 was first checked using the same uniform grid (2,092 equations) as that used for Fig. 7(*a*) and the result obtained, shown in Fig. 7(*b*), was essentially the same. Then a grid of varying element size, shown in Fig. 8 (with a singular element of size $h = 0.01a$), was introduced; the results obtained by the explicit algorithm are shown in Fig. 8. Accuracy in the average sense is improved, but a spurious high frequency oscillatory motion is superimposed on the solution; it becomes stronger with time and makes the results useless after the first peak (first diffraction of diffracted wave). Thus, the grid of varying element size has not brought the desired improvement. This is probably caused by spurious reflections from the boundaries between elements of different size. Further numerical examples for the plane wave propagation have been calculated and these spurious reflections have been found to be especially intense when the adjacent elements vastly differ in size. Thus, it was thought that the use of only small differences in the sizes of adjacent elements, as in Fig. 8, would eliminate this problem; but this only mitigated it, and not to a sufficient degree. This is probably due to the fact that spurious wave reflections, albeit small, occur on too many element boundaries in this system, and their energies accumulate. (However, for a nonlinear material, the energy of these spurious waves would be absorbed due to hysteresis making the solution less inaccurate.)

Difficulty Stemming from Loading of Crack Surface.—The fact that the solution in Fig. 7(*a*) does not approach the correct static value of K_3 suggests examining the static problem for a uniform traction applied at the crack surface [Fig. 4(*b*)]. The same static value of K_3 must be obtained as for an equal uniform traction applied at infinity [Fig. 4(*a*)]. However, when this case was computed

using the finite element grid shown in Fig. 5(*a*), the value of K_3 differed by about 12%. Since the difference between the two cases is a homogeneous strain field (cases c and d in Fig. 4), one must conclude that the singular crack tip elements [of Fig. 5(*a*) and Fig. 3] cannot adequately represent homogeneous strain states. This was confirmed by numerical results [see Table 1, Cols. 7-14). Curiously, this was also true of the crack-tip elements with free nodes, which include the homogeneous strain field.

In static problems without loading on the crack surfaces, a homogeneous *antiplane shear strain does not arise near the crack tip. In wave diffraction* problems, however, such a homogeneous strain field is inevitable in the formulation given herein, because the diffracted wave [solution w_B defined at the beginning, Fig. 1(*b*)] is caused by a loading on the crack surface. Therefore, a crack-tip element for wave diffraction problems must be able to represent correctly the states of homogeneous strain.

Dynamic Problem with Statically Calibrated Nonsingular Crack-Tip Elements

From the preceding analysis it becomes clear that singular crack-tip elements are only of limited usefulness in wave diffraction situations. This invites a more detailed exploration of the use of nonsingular crack-tip elements, which can represent homogeneous strain adequately. From extensive studies in static crack problems it is known (32) that, with nonsingular elements, the convergence with diminishing element size is much slower, the error being $O(\sqrt{h})$ rather than $O(h^2)$. The K_3 values obtained by matching the near-tip field to displacements by energy considerations or by the J integral (16), or by determining the energy release rate from two calculations for crack tip located at adjacent nodes (22), either are not accurate enough or are inapplicable to dynamics.

However, a simple remedy is possible by adopting a technique similar to the one recently proposed by Walsh (36,37) for static problems, although without the strong refinement of the grid in the vicinity of the crack tip, as considered by Walsh, and by extending this technique to dynamics. In this technique one ascertains in advance for a certain simple loading case the ratio R of the exact value of K_3 to the numerical value of the crack opening displacement w_c in the nearest node of the crack surface. The value of w_c may have a large error but this error happens to be nearly the same for various loadings. Thus, once the crack tip element is calibrated by calculating the ratio $R = K_3/w_c$, one may expect that nearly the same ratio will apply for other loadings. This has been numerically verified by Walsh (36,37) for static problems and it is postulated herein that the same holds for dynamic problems. For calibrating the crack-tip element, one may take, for example, either the field from Eq. 6 or the field from Eq. 9, apply the corresponding stresses at the finite element system boundary as the prescribed boundary tractions, and solve w_c by finite elements. In the dynamic problem, the time history of K_3 is then assumed to be given with a reasonable accuracy as

$$K_3(t) = R\,w_c(t) \quad (14)$$

This method of calculating $K_3(t)$ has been tried, choosing quite large nonsingular crack-tip elements, of size $h = a/8$. For such a large size it was possible to use constant-size finite elements throughout the whole grid, thus eliminating

spurious wave reflections at element boundaries and permitting the use of both the implicit and the explicit step-by-step algorithms. The numerical results obtained with the explicit algorithm are plotted in Fig. 9(*a*) and the shape of the crack opening in the static problem, used to determine the calibration factor, R, is also shown in Fig. 9(*a*). The numerical results are distinctly superior to those obtained previously with singular crack-tip elements, despite the use of a rather coarse grid, and they are obtained at a relatively very low cost of computer time. This corroborates the assumption made by Eq. 14.

A note on the small superimposed oscillatory motion is in order [Fig. 9(*a*)]. Such spurious motions behind the wave front have been observed before (14). It has also been suggested (14) that they can be eliminated by introducing small artificial damping. This has been tried in the present problem, using various values of damping proportional either to mass matrix or to stiffness matrix. It was found, however, that elimination of the small high-frequency oscillatory motion is impossible by means of artificial damping because the mean response is incorrectly distorted [see Fig. 9(*b*)]. However, it would probably be possible to eliminate these spurious motions by a filtering technique (17).

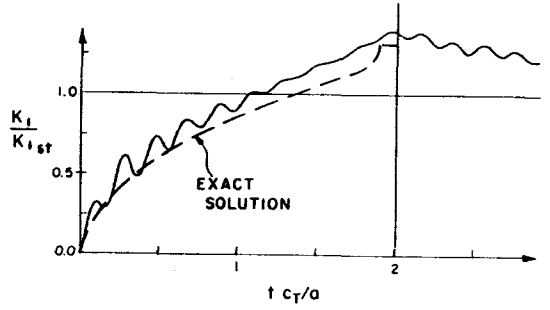

FIG. 10.—K_I History for In-Plane Problem by Explicit Method with Nonsingular Calibrated Crack-Tip Elements as Compared to Exact Elastodynamic Solution

It has also been accidentally noticed that the superimposed spurious high-frequency motion in Fig. 9(*b*) can be greatly reduced by using a grid in which all diagonals have one direction [Fig. 4(*b*)], instead of alternating directions shown in Fig. 5(*b*). However, it was not possible to recalculate all previous results with such a grid. Obviously, the grids for wave propagation should be as regular and repetitive as possible. The alternating diagonals in Fig. 5(*b*) have been used because it was thought that a grid with one-direction diagonals [Fig. 4(*b*)] introduces a nonisotropic directional bias. The opposite is the case, however, since the alternating diagonals give rise to a mass matrix that does not have equal lumped mass for adjacent nodes even when the grid is regular.

Extension to Planar Motion

The technique of statically calibrated ordinary crack-tip element has also been applied to in-plane motion. Constant pressure was suddenly applied to the crack surface and the history of mode I stress intensity factor K_I was calculated. The comparison with the exact solution (31) is favorable (see Fig. 10).

Conclusions

1. Crack-tip elements with a singular strain field are much less effective in wave propagation problems than they are in static ones. They are especially poor in wave diffraction. The reason is that they cannot accurately describe states of homogeneous strain induced by loading the crack surfaces.
2. By far most effective is a statically calibrated nonsingular crack-tip element that was proposed by Walsh for static problems and is extended herein to dynamics. The calibration is done on the basis of the ratio of crack opening displacement in the nearest node, obtained from a test calculation by finite elements for the chosen grid loaded at remote boundaries, to the exact stress intensity factor determined from the known exact static solution for the test case.
3. Implicit time-step algorithms are most accurate for time step $\Delta t \approx h/c_T$, which requires the sizes of all elements to be approximately the same.
4. The iterative solution of the implicit equation system for the time step is much more economical than the direct solution, because diagonal coefficients of equation matrix are large due to the mass matrix.
5. The explicit time step algorithm used, requiring a time step roughly 10 times smaller, is about equally economical and the need for equal element sizes is not so stringent. (However, the explicit algorithm is not possible when the mass or damping matrix is nondiagonal.)
6. The so-called nonreflecting boundary works only when the front of the incident wave is nearly planar within the region of the element and the angle of incidence is small ($\leq 15°$). When any two adjacent elements are of different size, spurious wave reflections occur at the boundary between such elements. The spurious high frequency motion superimposed on the correct solution cannot be removed by artificial damping, contrary to previous suggestions.
7. The lumped mass matrix gives more accurate results and smaller spurious superimposed oscillations than does the consistent mass matrix. This is particularly marked when a singular element is used.
8. In static problems, the singular crack-tip element with constrained nodes (7,35) gives best results for the stress intensity factor due to remote loading, but very poor displacements in the near nodes. Crack-tip elements with free nodes, which include both the singular and homogeneous strain fields, improve the displacement values but give poor results for the stress intensity factor.
9. All singular elements give rather inaccurate values of the stress intensity factor when the load is applied on the crack surface. Aside from wave diffraction, this fact happens to be also of interest for analyzing static hydraulic fracture of rock induced by pressurized water filling the crack.

Remark.—The case of wave with a discontinuous stress front, considered herein, is of course the most unfavorable situation for finite element calculations. If wave with a smooth front were considered, the results in Figs. 2 and 6-10 would undoubtedly exhibit smaller errors, and the difficulty mentioned in conclusion No. 3 would not be as severe.

Acknowledgment

The work of the second and third writers was carried out in the course of research sponsored by the National Science Foundation under Grant No. ENG

70-01465 A02 to Northwestern University, Evanston, Ill. Part of the work of the first writer on crack-tip elements for statics was supported under National Science Foundation Grant No. AER75-00187 to Northwestern University.

APPENDIX.—REFERENCES

1. Aamodt, B., and Bergan, P. G., "Numerical Techniques in Linear and Nonlinear Fracture Mechanics," *Computational Fracture Mechanics*, F. Rybicki and S. E. Benzley, eds., American Society of Mechanical Engineers, New York, N.Y., 1975, pp. 199-217.
2. Achenbach, J. D., "Brittle and Ductile Extension of a Finite Crack by a Horizontally Polarized Shear Wave," *International Journal of Engineering Science*, Vol. 8, 1970, pp. 947-966.
3. Achenbach, J. D., *Wave Propagation in Elastic Solids*, North Holland Publishing Co., Amsterdam, the Netherlands, 1973.
4. Anderson, J. C., and Gupta, R. P., "Earthquake Resistant Design of Unbraced Frames," *Journal of the Structural Division*, ASCE, Vol. 98, No. ST11, Proc. Paper 9344, Nov., 1972, pp. 2523-2539.
5. Anderson, G. P., Ruggles, V. L., and Stibor, G. S., "Use of Finite Element Computer Programs in Fracture Mechanics," *International Journal of Fracture Mechanics*, Vol. 7, 1971, pp. 63-76.
6. Bathe, K. J., and Wilson, E. L., "Stability and Accuracy Analysis of Direct Integration Methods," *Earthquake Engineering and Structural Dynamics*, Vol. 1, 1973, pp. 283-291.
7. Bažant, Z. P., "Singular Finite Element for Statics and Dynamics of Elastic Solids with Cracks and Notches," *Proceedings*, 10th Anniversary Meeting, *Paper TmB6*, Society of Engineering Sciences, Rayleigh, N.C., 1973.
8. Benzley, S. E., "Representation of Singularities with Isoparametric Finite Elements," *International Journal of Numerical Methods in Engineering*, Vol. 8, 1974, pp. 537-545.
9. Benzley, S. E., and Beisinger, Z. E., "Chiles-A Finite Element Computer Program that Calculates the Intensities of Linear Elastic Singularities," *Report No. S2A-73-0894*, Sandia Laboratories, Albuquerque, N.M., 1973.
10. Benzley, S. E., and Parks, D. M., "Fracture Mechanics," *Structural Mechanics Computer Programs*, W. Pilkey, et al., eds., University Press of Virginia, Charlottesville, Va., 1974.
11. Bergan, P. G., and Aamodt, B., "Finite Element Analysis of Crack Propagation in Three-Dimensional Solids under Cyclic Loading, "*Nuclear Engineering and Design*, Vol. 29, 1974, pp. 180-188.
12. Byskov, E., "The Calculation of Stress Intensity Factors Using the Finite Element Technique," *International Journal of Fracture Mechanics*, Vol. 6, 1970, pp. 159-167.
13. Chen, S. K., Tuba, I. S., and Wilson, W. K., "On the Finite Element Method in Linear Fracture Mechanics," *Engineering Fracture Mechanics*, Vol. 2, 1970, pp. 1-18.
14. Fu, C. C., "A Method for the Numerical Integration of the Equations of Motion Arising from a Finite Element Analysis," *Journal of Applied Mechanics*, American Society of Mechanical Engineers, Sept., 1970, Vol. 37, pp. 599-605.
15. Hildebrand, F. B., *Finite-Difference Equations and Simulations*, Prentice Hall, Inc., Englewood Cliffs, N.J., 1968, pp. 235-236.
16. Hilton, P. D., and Sih, G. C., "Applications of the Finite Element Method to the Calculation of Stress Intensity Factors," *Methods of Analysis and Solutions of Crack Problems*, G. C. Sih, ed., Noordhoff International Publishers, Leyden, the Netherlands, 1973.
17. Holmes, N., and Belytschko, T., "Postprocessing of Finite Element Transient Response Calculations by Digital Filters," *Technical Report*, Department of Materials Engineering, University of Illinois at Chicago Circle, Chicago, Ill., 1975.
18. Lysmer, J., and Kuhlemeyer, R. L., "Finite Dynamic Model for Infinite Media," *Journal of the Engineering Mechanics Division*, ASCE, Vol. 95, No. EM4, Proc. Paper 6719, Aug., 1969, pp. 859-877.
19. MacNeal, R. H., and McCormick, C. W., "The Nastran Computer Program for Structural Analysis," *Computers and Structures*, Vol. 1, 1971, pp. 389-412.

20. Morley, L. S. D., "A Finite Element Application of the Modified Rayleigh-Ritz Method," *International Journal for Numerical Methods in Engineering*, Vol. 2, 1970, pp. 86-98.
21. Morley, L. S. D., "Finite Element Solution of Boundary Value Problems with Non-removable Singularities," *Royal Aircraft Establishment Technical Report 73034*, London, England, Apr., 1973.
22. Mowbray, D. F., "A Note on the Finite Element Method in Linear Fracture Mechanics," *Engineering Fracture Mechanics*, Vol. 2, 1970, pp. 173-176.
23. Newmark, N. M., "A Method of Computation for Structural Dynamics," *Journal of the Engineering Mechanics Division*, ASCE, Vol. 85, No. EM3, Proc. Paper 2094, July, 1959.
24. Oglesby, J. J., and Lomacky, O., "An Evaluation of Finite Element Methods for the Computation of Elastic Stress Intensity Factors," *Journal of Engineering for Industry*, American Society of Mechanical Engineers, Vol. 95, 1973, pp. 177-185.
25. Pian, T. H. H., Tong, P., and Luk, C. H., "Elastic Crack Analysis by a Finite Element Hybrid Method," *Preprints*, 3rd Conference on Matrix Methods in Structural Mechanics, Wright-Patterson Air Force Base, Ohio, 1971.
26. Rao, A. K., Raju, R. S., and Krishna Murty, A. V., "A Powerful Hybrid Method in Finite Element Analysis," *International Journal for Numerical Methods in Engineering*, Vol. 3, 1971, pp. 389-403.
27. Ravera, R. J., and Sih, G. C., "Transient Analysis of Stress Waves Around Cracks under Antiplane Strain," *The Journal of the Acoustical Society of America*, Vol. 47, No. 3, 1970, pp. 875-881.
28. Rice, J. S., and Tracey, D. M., "Computational Fracture Mechanics," *National Aeronautics and Space Administration Technical Report NGL40-002-080/7*, Division of Engineering, Brown University, Providence, R.I., 1971.
29. Sneddon, I. N., and Lowengrub, M., *Crack Problems in the Classical Theory of Elasticity*, John Wiley and Sons Publishing Co., Inc., New York, N.Y., 1969.
30. Swanson, S. R., "Finite-Element Solutions for a Cracked Two-Layered Elastic Cylinder," *Engineering Fracture Mechanics*, Vol. 3, 1971, pp. 283-290.
31. Thau, S. A., and Lu, T. H., "Transient Stress Intensity Factors for a Finite Crack in an Elastic Solid Caused by a Dilatational Wave," *International Journal of Solids and Structures*, Vol. 7, 1971, pp. 731-750.
32. Tong, P., and Pian, T. H. H., "On the Convergence of the Finite Element Method for Problems with Singularities," *International Journal of Solids and Structures*, Vol. 9, 1973, pp. 313-321.
33. Tracey, D. M., "Finite Elements for Determination of Crack Tip Elastic Stress Intensity Factors," *Engineering Fracture Mechanics*, Vol. 3, 1971, pp. 255-266.
34. Tracey, D. M., "Finite Elements for Three-Dimensional Elastic Crack Analysis," *Nuclear Engineering and Design*, Vol. 26, 1974, pp. 282-290.
35. Walsh, P. F., "The Computation of Stress Intensity Factors by a Special Finite Element Technique," *International Journal of Solids and Structures*, Vol. 7, 1971, pp. 1333-1342.
36. Walsh, P. F., "Stress Intensity Factors by Calibrated Finite Element Method," *Journal of the Engineering Mechanics Division*, ASCE, Vol. 98, No. EM6, Proc. Paper 9396, Dec., 1972, pp. 1611-1614.
37. Walsh, P. F., "Linear Fracture Mechanics in Orthotropic Materials," *Engineering Fracture Mechanics*, Vol. 4, 1972, pp. 533-541.
38. Wilson, E. L., "Elastic Dynamic Response of Axisymmetric Structures," *Report No. 69-2*, Structural Engineering Lab, University of California, Berkeley, Calif., 1969.
39. Yamamoto, Y., "Finite Element Approaches with the Aid of Analytical Solutions," *Recent Advances in Matrix Methods of Structural Analysis and Design*, University of Alabama Press, Huntsville, Ala., 1971, pp. 85-103.
40. Yamamoto, Y., and Tokuda, N., "Determination of Stress Intensity Factors in Cracked Plates by the Finite Element Method," *International Journal for Numerical Methods in Engineering*, Vol. 6, 1973, pp. 427-439.

12220 FE ANALYSIS OF WAVE DIFFRACTION BY A CRACK

KEY WORDS: **Cracks; Diffraction; Engineering mechanics;** Finite element method; Stress measurement; **Wave dispersion**

ABSTRACT: The time history of mode III stress intensity factor K_3 is calculated, and compared with exact solutions. It is found that crack-tip elements with a singular strain field are much less effective in elastodynamics than elastostatics. The nonsingular (ordinary) crack tip element whose crack-opening displacement is calibrated against the exact value of k_3 by means of a static finite element solution for load applied at remote boundaries was found to be most effective. Detailed studies have also been carried out for implicit and explicit time-step algorithms; proper sizes of elements; methods for solving equation systems; the questions of nonreflecting boundary; lumping of mass matrix; and elimination of spurious oscillations superimposed on the correct solution. The convergence and accuracy of various singular crack-tip elements have been examined. Finally, application of the technique for in-plane motions is also presented.

REFERENCE: Bazant, Zdenek P., Glazik, John L., Jr., and Achenbach, Jan D., "Finite Element Analysis of Wave Diffraction by a Crack," *Journal of the Engineering Mechanics Division,* ASCE, Vol. 102, No. EM3, **Proc. Paper 12220**, June, 1976, pp. 479-496